ELSEVIER

Journal of Power Sources 76 (1998) 1–10

JOURNAL OF POWER SOURCES

Lithium insertion in ball-milled graphite

C.S. Wang [a,*], G.T. Wu [b], W.Z. Li [b]

[a] *Department of Materials Science and Engineering, Zhejiang University, Hangzhou 310027, China*
[b] *Department of Physics, Zhejiang University, Hangzhou 310027, China*

Received 27 April 1998; accepted 11 May 1998

Abstract

The effects of mechanical milling on the microstructure, morphology and electrochemical performance of graphite powders with respect to lithium insertion are studied. After 150 h of ball-milling, the well-graphitized graphite has been pulverized into small particles with a size of about 50 nm, in which there are a lot of excess vacancies, microcavities and metastable carbon interstitial phases with sizes around 13 Å. Due to the large surface energy, the merging of single particles is favoured and results in the formation of agglomerates with average size about 1 μm. Voids are formed among the agglomerated particles. The ball-milled graphite shows reversible specific capacity for lithium of 700 mA h g^{-1} ($L_{1.88}C_6$) with large hysteresis. The large reversible capacity is due mainly to Li doping at vacancies, microcavities (or at the edges of the metastable carbon interstitial phase) and voids. The bonding change between the interstitial carbon and the carbon in the aromatic plane that is induced by insertion of Li atoms leads to hysteresis. During charge–discharge cycles, the reversible capacity above 1 V decreases rapidly, which may be due to some vacancies and microcavities being annihilated by moveable and some bound interstitial carbon and to electrolyte penetrating gradually into voids formed by agglomerated particles during the Li insertion and desertion process.

Keywords: Electrochemical performance; Graphite; Ball-milling; Specific capacity; Lithium-ion battery

1. Introduction

Research and development is in progress world-wide to produce advanced anode materials for use in lithium-ion rechargeable battery technology. Much of this effort is focused on developing various carbonaceous materials [1–3]. Graphite, because of its ability to intercalate both rapidly and reversibly one lithium per six carbons (leading to a capacity of 372 mA h g^{-1}) at a potential < 0.5 V vs. Li, is presently used as the anode material in lithium-ion batteries.

Recently, there have been numerous reports of carbonaceous materials with capacities which greatly exceed that of graphite, such as heat-treated polyfurfuryl alcohol [4], polyparaphenylene [5], mesophase pitch [6,7], phenolic resin [8,9], phenolic resins with cross-linking agent [10,11], oxided epoxy resins [12], and ball-milled graphite and coke [13]. To explain this phenomenon, Sato et al. [5] proposed that lithium can occupy nearest neighbour sites between graphene layers. This explanation would require, however, a mechanism for the lithium ions to overcome the large screened coulomb repulsion between ions on nearest-neighbor sites in the absence of a huge applied pressure on the lithium [14]. Moreover, the fact that the peak wave number of the E_{2g2} band of mesocarbon microbeads heated at 700°C does not shift at all over the whole potential range indicates that the high capacity of disordered soft carbon (MCMB) does not originate from lithium insertion between organized graphene layers, but from lithium doped into the region without an organized graphitic structure [15]. Dahn et al. [14] and Zheng et al. [9,16] claim that lithium can bind near hydrogen atoms in carbonaceous materials containing substantial hydrogen; the voltage profile with large hysteresis for carbonaceous materials is related to the hydrogen in these samples. On the other hand, ball-milled graphite and coke containing no hydrogen also exhibit high capacity with large hysteresis [13]. Mabuchi et al. [6] and Tokumitsu et al. [10] have suggested that lithium can insert into microcavities within the carbonaceous materials. Recently, Xiang et al. [11] proposed that, except for the lithium intercalated between graphene layers, lithium is doped mainly at the edges of graphene

* Corresponding author. Fax: +86-571-795-11-52; E-mail: msecwang@dial.zju.edu.cn

0378-7753/98/$19.00
PII: S0378-7753(98)00114-1

layers, and that the interaction between lithium and atoms at the edges leads to a plateau at about 1 V. Although many models have been proposed, the mechanism for intercalation of lithium into disordered carbon is still not entirely clear. Detail studies on relationship between structural characteristics and electrochemical performances are needed.

Mechanical ball-milling has been shown to be a powerful technique to produce particles of controlled-size and with a homogeneous structure. Recently, it has been discovered that mechanical ball-milling can be used to obtain crystal-to-amorphous and/or crystal-to-nanocrystalline transitions for C [17,18] elements. A ball-milled graphite and soft carbon can reversibly intercalate two lithium per six carbon (e.g., Li_2C_6) while having 1 V voltage hysteresis [13]. In the present work, the morphology and structural characteristics of ball-milled graphite are monitored by using X-ray diffractometry (XRD), Raman spectroscopy, high-resolution electron microscopy (HREM), and transmission electron microscopy (TEM). It is then hoped to relate the structure of ball-milled graphite to its electrochemical behaviour for lithium insertion and desertion.

2. Experimental

2.1. Preparation of ball-milled graphite

Milling was carried out in a conventional planetary ball mill. Pure graphite (99.9%, 325 mesh) was put into a hard-bearing steel vial under a dry, pure argon atmosphere. The steel vial was sealed with an elastomer 'O' ring seal. The ball milling was performed for 150 h without interruption. The weight ratio of steel ball to graphite powder was 12:1. The rotation rate of the vial was 270 rpm.

2.2. X-ray diffraction and raman spectra measurements

The structure of ball-milled graphite powders was analyzed by XRD measurements using a Philips PW1710 diffractometer with Cu $K_{\alpha 1}$ radiation (1.5418 Å). The crystallite size, L_c, was determined from the 002 carbon Bragg peak using the Scherrer equation [19], i.e.,

$$L_{hkl} = 0.9\lambda/(\beta\cos\theta)$$

where: λ is the X-ray wavelength; θ is the Bragg angle; β is the real half-peak width in radians after corrections for instrument broadening. The full-width at half intensity, β_{exp}, was first measured, and then the instrumental broadening, β_{inst}, was subtracted ($\beta = \sqrt{\beta_{exp}^2 - \beta_{inst}^2}$) to obtain β. The Raman spectra (RS) were excited with 150 mW of 5145 nm radiation from an argon ion laser, and the scattered light was dispersed with a V1000 ISA double spectrometer. The sample geometry for the RS measurements was a disk with a diameter of 3 mm and a thickness of 0.5 nm prepared by pressing the powder under a nominal pressure of 3.1 GPa.

2.3. HREM and TEM observations

The microstructure and morphology observations were performed by means of a side-entry JEOL2010 HREM with a point-to-point resolution of 0.19 nm, as well as by means of a JEOL200CX TEM. The powders prepared for HREM and TEM observations were first dispersed in alcohol and then placed on carbon-coated copper grids.

2.4. Electrochemical testing

All electrochemical measurements were carried out using coin-type test cells. Polytetrafluoroethylene (PTFE) diluted in anhydrous alcohol was added to the powder samples such that approximately 8 wt.% of the final electrode mass was PTFE. Excess anhydrous alcohol was added until the slurry reached a smooth, syrupy viscosity. The slurry was then spread uniformly on preweighed nickel foam. Once the electrode was dried, it was compressed between flat plates to $\sim$30 bar pressure and dried at 150°C under vacuum overnight, and then weighed to determine the active mass of carbon. The electrodes usually had an active mass of 16 mg. A microporous separator film, which had been wetted with 1 M $LiClO_4$ dissolved in a 50/50 (v/o) mixture of ethylene carbonate (EC) and diethyl carbonate (DEC), was sandwiched between the working electrode and a lithium metal foil anode. The electrode was then wet with the same electrolyte as the separator. Half cells were assembled in an argon-filled glove box. During the first three charge–discharge cycles, the electrode was cycled using a constant current of 15 mA g^{-1} between 0.005 and $\sim$2.8 V. To determine cycle life, a small potential range of 0.005 to $\sim$1.5 V was adopted during the charge/discharge cycles, and a cycling current of 15 mA g^{-1} was used in cycles 1–3, 10, and 20. A more-rapid cycling current of 45 mA g^{-1} was used for cycles 4–9 and 11–19.

3. Results and discussion

3.1. Structure analysis of ball-milled graphite

The XRD patterns for pristine graphite and ball-milled graphite are shown in Fig. 1. The graphite is a very well-graphitized graphite. The graphite stacked form is called hexagonal or 2H graphite. The peaks are very sharp and indicate a high crystallinity with crystallite sizes larger than 1000 Å. After 150 h of ball-milling, we observe a decrease in intensity as well as a broadening of the [002] carbon Bragg peak. The position of the [002] carbon Bragg peak is downshifted. L_c is 1.3 nm, which suggests that the

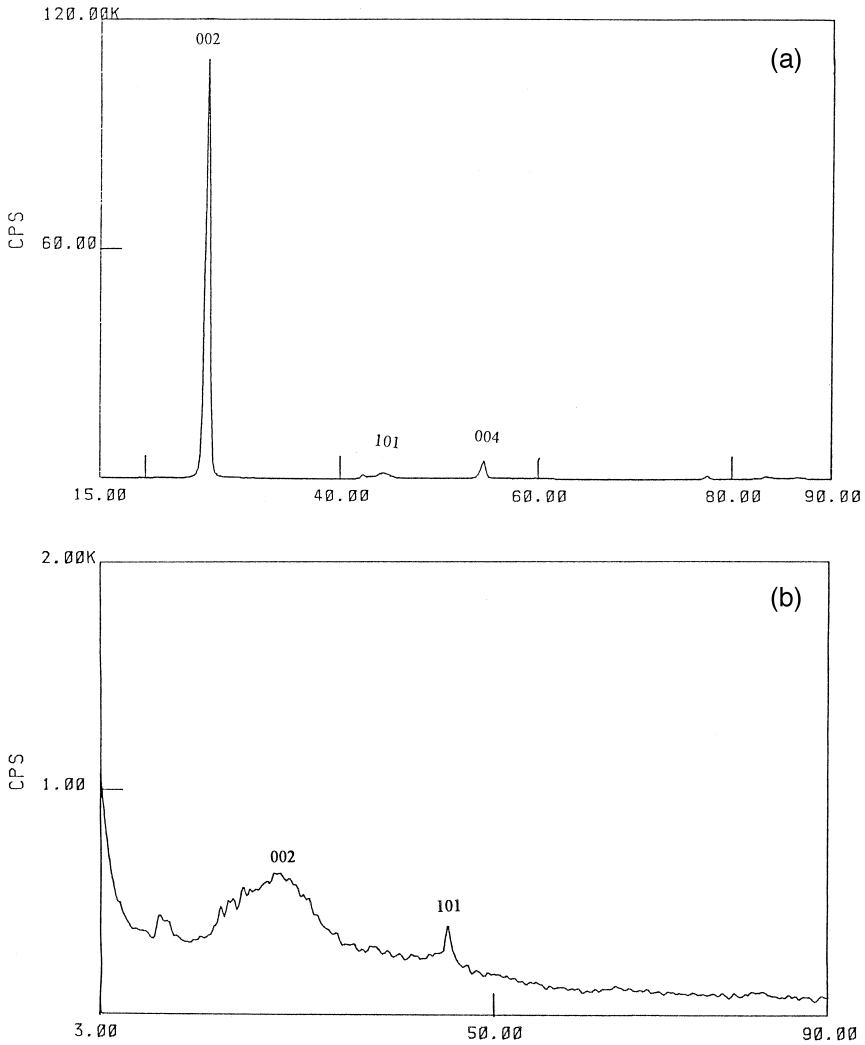

Fig. 1. XRD patterns for (a) pristine graphite, and (b) graphite ball-milled for 150 h.

average crystallite is about four unit cells thick. The interlayer distance (d_{002}) increases from 3.35 Å for pristine graphite to 3.55 Å for ball-milled graphite. The values of L_c and d_{002} are consistent with those of L_c and d_{002} for ball-milled graphite reported by Aladekomo and Bragg [20]. The present d_{002} is smaller, however, than the result ($d_{002} = 3.68$) of Shen et al. [17], but larger than the result ($d_{002} = 3.37$ Å) of Disma et al. [13]. The possible interpretation is that the milling rate may vary considerably according to the nature of the ball-mill, the speed, the charge, etc. [21]. The milling rate may increase in the following order:

(i) 8:1 ball-to-powder ratio and 65 h of milling time [13];

(ii) 12:1 ball-to-powder ratio, 270 rpm and 150 h of milling time (present work);

(iii) 40:1 ball-to-powder ratio, 720 rpm and 40 h of milling time [17].

It is reasonable to conclude that a high milling rate would result in a large d_{002} value.

Aladekomo and Bragg [20] found that, in mechanical milling of graphite, the increase in the interlayer spacing is in the step [20], and they asserted that the increase in d_{002} is attributed to the introduction of interstitial carbon atoms into the initial pristine graphite structure; the interstitial carbon atoms are between the aromatic planes of carbon atoms [18]. In mechanical ball-milling, the graphite initially forms a solid solution with single C_1 carbon [22] and then transforms to the metastable carbon interstitial phases characterized by spacings of 3.375, 3.4, 3.44 and 3.55 Å, which is similar to graphite intercalation compound (GIC) [20]. The steps in the interlayer spacing are also observed in the annealing of artificial carbon [23], in fast-neutron irradiation of graphite [24], which demonstrates the existence of interstitial carbon atoms between the aromatic planes of carbon atoms in these materials [25]. Therefore, we conclude that after 150 h of mechanical milling, the graphite has been transformed to metastable carbon interstitial phases and its structure is identical with those of carbonaceous materials obtained in pyrolyzing hydrocar-

bon [18]. Furthermore, the low intensity as well as a broadening of [002] Bragg peak after 150 h of ball-milling indicate that some defects, such as vacancies, vacancy line and loops, are also induced by mechanical milling.

Lattice defects in graphite break down the hexagonal symmetry of the graphite lattice and modify the optical selection rules for the lattice vibrational modes which can be observed in Raman scattering [26]. A single Raman line is theoretically expected for the hexagonal lattice of graphite and has been observed at around 1580 cm^{-1} in natural graphite and stress-annealed pyrolytic graphite. An additional Raman line is observed around 1360 cm^{-1} in glassy carbon, polycrystalline graphite and the lattice-defects graphite induced by mechanical milling [17,27]. The Raman line at 1360 cm^{-1} has been assigned to a vibrational mode that originates from the disorganized region near crystal edges and lattice defects [17]. The Raman spectra of pristine graphite and ball-milled graphite are shown in Fig. 2. The original graphite exhibits an intense graphite band at 1580 cm^{-1}. The 1360 cm^{-1} band also appears very weakly in this sample and suggests the existence of structural defects which may have been introduced in the course of sample preparation. In this case, the original graphite sample is milled for a very short time for X-ray diffraction measurements prior to Raman studies. After 150 h of milling, the increase in intensity of the 1360 cm^{-1} band is observed, which indicates that some lattice defects such as lattice vacancies are introduced into the ball-milled graphite. As is obvious from Fig. 2, another Raman band at 1620 cm^{-1} is clearly seen in the graphite ball-milled for 150 h. These RS results are in agreement with those of Nakamizo et al. [27] and Nikiel and Jagodzinski [28], who have found that the intensity of the 1620 cm^{-1} band increases with milling time, but that the exact nature of this Raman band is not clear. We believe that the 1620 cm^{-1} arises from the vibration of carbon–carbon atoms near an interstitial carbon atom, since the latter is bound to one plane and the atoms in the graphite plane are attracted towards the interstitial [22], which may increase the carbon–carbon bonds in the plane in the vicinity of interstitial, and if the force constant of the carbon–carbon bonds becomes larger then the 1580 cm^{-1} graphite band will shift towards the higher frequency side [27]. Since the number of interstitial carbon atoms between the aromatic planes of the carbon atoms increases with ball-milling time, the intensity of the 1620 cm^{-1} band increases with the ball-milled time [27]. Therefore, the Raman study on ball-milled graphite reconfirmed the intercalation of carbon atoms into graphite, which is suggested by XRD analysis. The Raman band at 1620 cm^{-1} has also been observed in carbon films prepared by plasma-enhanced chemical vapour deposition (PECVD) methods [29], and in ion-etched compression-annealed pyrolytic carbon [30]. Furthermore, the peak wavenumber of the E_{2g2} band for heated mesocarbon microbeads (MCMBs) shifts upwards from 1580 to 1600 cm^{-1} with decrease heat-treatment temperature from 2800 to 700°C [15] and may also be associated with the existence of interstitial carbon atoms between the aromatic planes of carbon atoms in MCMBs heated at 700°C.

3.2. Microstructure observation of ball-milled graphite

Bright-file HREM images of pristine graphite and ball-milled graphite are shown in Fig. 3. The original graphite is a well crystalline material (Fig. 3a). After 150 h of ball-milling, the well-graphitized graphite is pulverized to small particles, in which there are many basic structural units (BSU) with sizes of about four unit cells thick and 1.4 nm of lateral extent of graphite sheet (arrow a). In

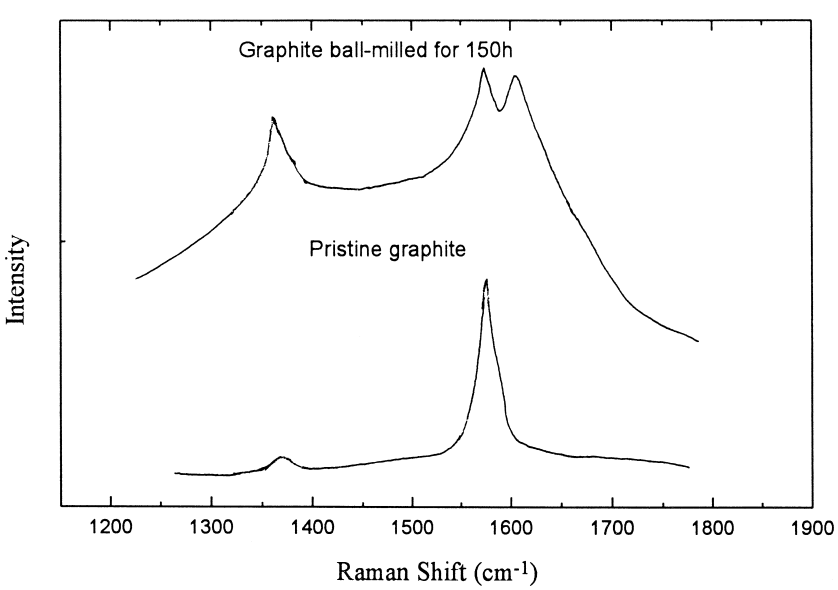

Fig. 2. Raman spectra for pristine (unmilled) graphite and ball-milled graphite.

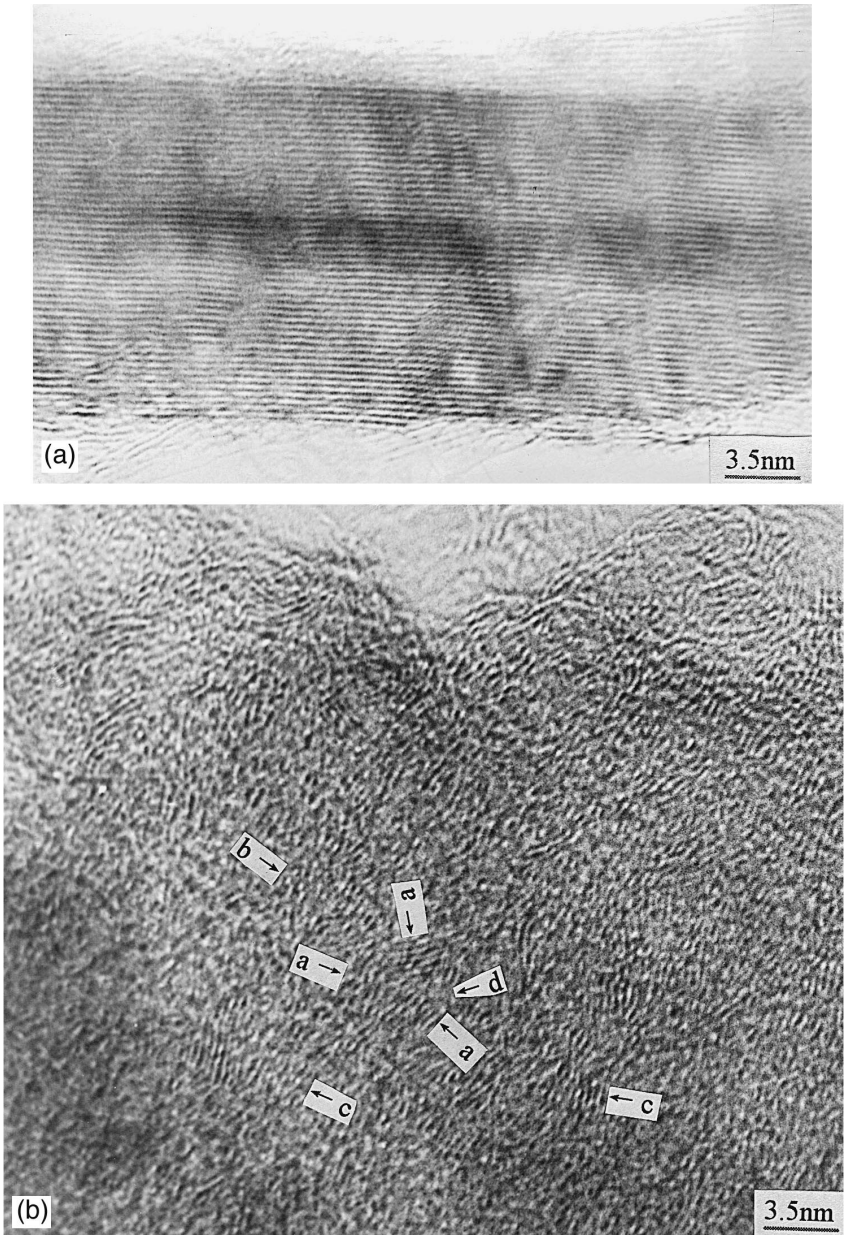

Fig. 3. HREM images for (a) pristine graphite and (b) ball-milled graphite.

lattice images of [002] reflections, the layers are wrinkled and have irregular thickness and a distribution of interlayer spacings. The wrinkled layers can be attributed to carbon interstitial atoms. This is because the atoms in the graphite plane are attracted towards the interstitial, but the nearest neighbours are force in the opposite direction [22]. Dislocation loops are observed, thought to be a regular 'raft' of interstitial atoms (arrow b), and may consist of loosely linked interstitial atoms each over or under the ring in adjacent layers [22]. Some of the BSUs are associated into distorted columns where they pile up much like bricks thrown into a heap (arrow c), that is, they tend to pile up approximately parallel but independently. 'Unorganized carbon' which may consist of bulked single layers or tetrahedrally bonded carbon [31] exist between the misoriented BSUs (arrow d), and microcavities can be formed at the edge of the BSUs and in region of unorganized carbon [6,10]. The microstructure of graphite ball-milled for 150 h is similar to that of pitch coke heated at 800°C [32].

3.3. Morphology analysis of ball-milled graphite

TEM images of pristine graphite and ball-milled graphite are presented in Fig. 4. From graphite fractures before and after 150 h of ball-milling, we observe a decrease in size (an average mean diameter 50 nm) and lamella particles are produced with an average mean diameter of about 1 μm and a thickness of about 0.6 μm. Voids are formed among the particles.

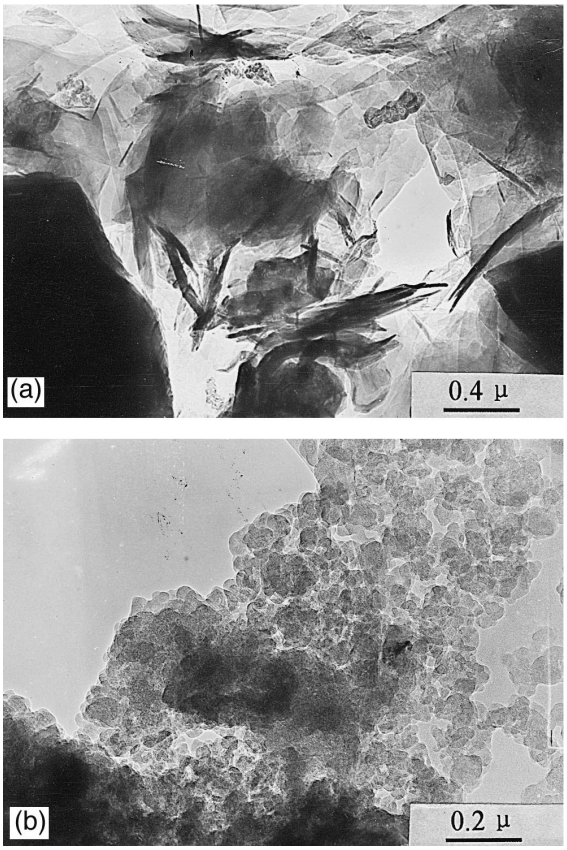

Fig. 4. TEM images for (a) pristine graphite and (b) ball-milled graphite.

3.4. Charge and discharge of ball-milled graphite electrode

Fig. 5 shows the first charge (lithium insertion) and subsequent charge–discharge of pristine graphite and ball-milled graphite. The potential profile is slanted for ball-milled graphite and flat for pristine graphite. The reversible and irreversible capacity of pristine graphite is about 300 and 125 mA h g^{-1}, respectively. After 150 h of ball-milling, the reversible capacity increases up to 700 mA h g^{-1} which corresponds to 1.88 Li for 6C, which is about twice that of pristine graphite. Further, this reversible capacity displays large potential hysteresis (Li is inserted near 0 V but is removed at about 1 V vs. Li). Also, the irreversible capacity increases up to 580 mA h g^{-1}. The large irreversible capacity at about 0.8 V is believed to be due to the electrolyte decomposition that results in the formation of a passivating film or solid electrolyte interphase (SEI) on the ball-milled graphite surface with larger surface area [13]. These results are similar to those reported by Disma et al. [13] for milled graphite. These authors concluded that large amounts of lithium are being inserted on both surfaces of the single-layer carbon as induced by ball-milling. Our work here shows, however, that ball-milled graphite offers little evidence of single-layer carbon. Moreover, such an explanation would require the chemical potential of the inserted lithium to be very close to that of metallic lithium, because it would be weekly bound to the carbon, and no hysteresis would be expected. The large reversible capacity with 1 V of potential hysteresis is also observed in carbonaceous materials containing H[9]. Dahn et al. [14] argue that a hydrogen atom can bind a lithium atom in hydrogen-containing carbons and that the inserted lithium can transfer part of its 2s electron to nearby hydrogen, which can lead to excess reversible capacity and hysteresis. The PVC550 and CRO580 samples in Ref. [16] and carbons prepared from phenolic resins [11] depart significantly, however, from the solid line of one Li per H. The reversible capacities of PPS and ENR samples are independent of the H:C content [16] and ball-milled graphite containing no hydrogen atoms also displays a similar reversible capacity and potential profile to carbonaceous materials containing hydrogen atoms [13]. Furthermore, in a massive review of ternary graphite–alkali–hydrogen compounds, Enoki et al. [33] show that since lithium has a strong affinity for hydrogen, the inserted lithium would react with hydrogen and form a mixture of C and LiH. Matsumura et al. [7] have confirmed that there is a significant amount of Li remaining in discharged mesophase pitch prepared at lower heat treatment temperatures (HTTs) and residual lithium exists as a stable compound. Stable compounds are formed at some active sites, in the bulk of carbon electrode. Matsumura et al. [7] attributed these active sites to –OH and carbon radicals, but we consider the active sites to be C–H. Inserted lithium can react with these C–H active sites to form stable compounds, HLi. From XPS measurements of discharged mesophase pitch heated at low HTTs, Matsumura et al. [7] also found that the binding energy of lithium remaining in the bulk of the discharged sample is 54.9 eV, which is ~2.5 eV higher than that of metallic lithium (52.5 eV) and ~0.25 eV lower than that of Li_2CO_3 on the surface. The 54.9 eV may be assigned to the binding energy of Li(1s) for HLi. Recently, Xing and Dahn [34] reported that when a sugar carbon electrode is exposed to air for 8 days, two capacity peaks (located near 0.8 and 0.3 V) are observed in the first lithium insertion

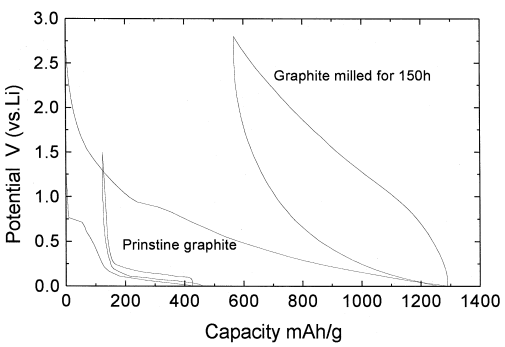

Fig. 5. First charge and second charge–discharge for pristine graphite and ball-milled graphite.

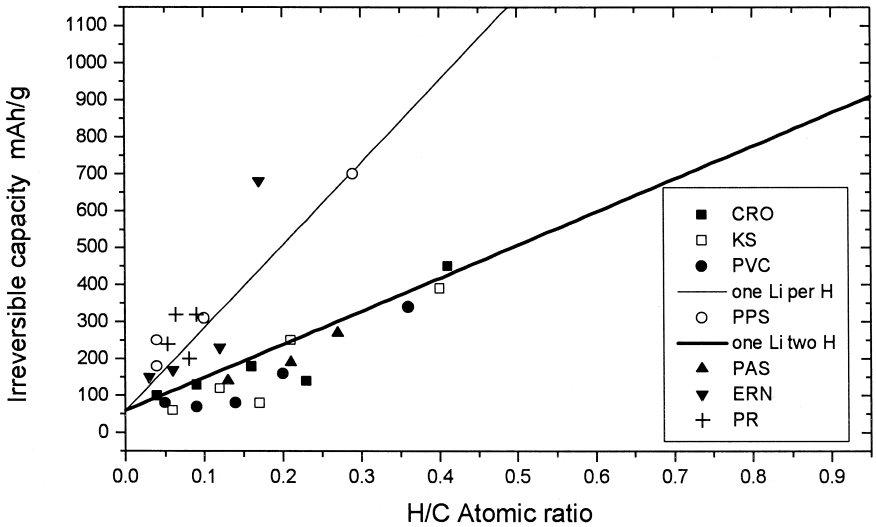

Fig. 6. Irreversible capacity of carbonaceous materials plotted as a function of their hydrogen content. Data for PAS (polyacenic semiconductor) and PR (phenolic resin) are reported in Refs. [8,11], respectively. The other data are reported in Ref. [16]. The thin solid line assumes that each hydrogen atom can bind with one lithium atom, and the thick solid line represents two hydrogen atoms binding to one lithium atom.

derivative curve. The peak located near 0.8 V is related to the formation of Li_2CO_3, LiOH, Li_2O and $(CH_2OCO_2Li)_2$ [35], the peak at 0.3 V may be due to the formation of HLi, since the potential for the oxidation of lithium is higher than that for the formation of lithium hydride [36]. Xing and Dahn [34] found the peak intensity at 0.6 to $\sim$1.1 V increases and no peak at about 0.3 V is observed when the sugar carbon electrode is exposed to CO_2 (10 min) or O_2 (2 h). When sugar carbon is exposed to water steam (100°C) or air for long time, however, a major capacity peak near 0.3 V in the first lithium insertion derivative curve can be clearly seen. This is because the long exposure time may allow C–H functional groups to form. Moreover, the fact that the formation of a stable compound causes the irreversible capacity [7] and that the irreversible capacity increases with the H:C ratio [16] confirms again that the stable compound is HLi. Therefore, we conclude that the inserted lithium reacts with hydrogen and forms the stable compound HLi, and that this compound causes additional irreversible capacity. To confirm this assumption, we examined the published work in Refs. [8,11,16], and noticed that the irreversible capacity of the materials under study displayed a linear dependence on the H:C atomic ratio of the sample, as shown in Fig. 6. The thick and thin solid lines in this figure are the theoretical capacity if one hydrogen atom can bind a Li atom and two hydrogen atoms can bind one lithium atom, respectively, and if the irreversible capacity due to solvent decomposition is 60 mA h g^{-1} [34]. Above 60 mA h g^{-1}, there is a striking dependence of the irreversible capacity on the H:C ratio. Each hydrogen atom binds a lithium atom and forms HLi in PPS, ERN and PR [11] samples, but appears that two hydrogen atoms bind a lithium atom in CRO, KS, PVC and PAS [8]. The reason is not clear at present, but may be related to a difference in the structure of the two groups of carbon materials. Recently Xiang et al. [11] proposed a new mechanism, in which they proposed that lithium is doped mainly at the edges of the graphite layer and that the interaction between lithium and atoms at the edges leads to the plateau at $\sim$1 V vs. Li/Li^+. This mechanism is similar to the 'microcavities mechanism' proposed by Tokumitsu et al. [10] and Mabuchi et al. [6], since most microcavities may be formed at the interface between BSU and the unorganized carbon region. The strong bond between lithium and atoms at the edges leads to lithium doping only at a high potential, however, and does not induce potential hysteresis. Inaba et al. [15] have reported that the intensity of the A_{1g}, which reflects the vacancy defects in the plane and the disorganized region near crystal edges, changes by about 300 mV to 1.9 V during the lithium insertion and de-insertion process, and no potential hysteresis appears. This indicates that lithium insertion and de-insertion into/from vacancies is at a higher potential than that between interlayers, and that the bond between lithium and atoms at the edges does not lead to potential hysteresis in the charge–discharge process.

From above analysis, it is concluded that hydrogen atoms in carbonaceous materials cannot cause the excess reversible capacity and potential hysteresis, but results in irreversible capacity. During lithium insertion, the lithium atoms can be doped in the vacancies, microcavities, or at the edges of graphite layers, but this does not lead to potential hysteresis.

3.5. Mechanism for charge–discharge reaction of ball-milled graphite

We propose a new mechanism for the charge–discharge reaction of ball-milled graphite. This mechanism is illustrated in Fig. 7.

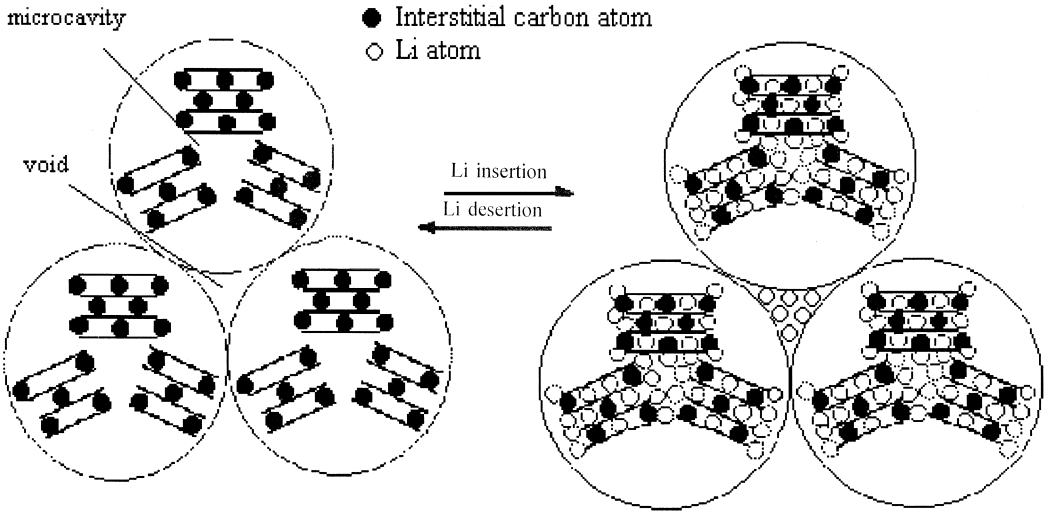

Fig. 7. Schematic illustration of lithium insertion/de-insertion mechanism in ball-milled graphite.

From XRD, Raman and HREM analyses, it is thought that, after 150 h of ball-milling, the well-graphitized graphite with crystallite size larger than 1000 Å has been pulverized into small particles with size 50 nm. In these particles, there are many excess (non-equilibrium) vacancies, microcavities and metastable carbon interstitial phases with size about 13 Å, which we term the basic structure unit (BSU). As noted above, some of the BSUs are associated into distorted columns where they pile up much like bricks thrown into a heap. The microcavities are formed between the BSUs. Since the larger surface energy favours the merging of single particles (with an average mean diameter of 50 nm), agglomerates with size about 1 μm are formed and voids exist among the particles. During charge, lithium species intercalate into the interlayer of the BSUs, diffuse through the interstitial carbon atoms, and finally are doped into the vacancies and microcavities [6,10] or at the edges of the BSU layers [11]. Also, some lithium species may intercalate into interlayers in the neck region which connects two primary particles and dope into the voids formed by agglomerated particles, since the reversible capacity increases with the extent of agglomeration [37]. During discharge, lithium species first de-intercalate to a certain extent from the BSUs and then are undoped from the vacancies, microcavities, voids or the edges of the BSU layers. Since many interstitial carbon atoms reduce the amount of lithium insertion between the interlayer of the BSUs, most of the reversible capacity is due to lithium storage in the vacancies, microcavities [6,10], voids [37], or the edges of the BSU layers [11]. This has been confirmed by an in situ Raman study of the electrochemical insertion of lithium into mesocarbon microbeads heated at 700°C [15]. Inaba et al. [15] found that the peak wavenumber of the E_{2g2} band of MCMB700, which consists mainly of metastable carbon interstitial phases [20], does not shift at all over the whole potential range. Because the interstitial carbon atoms bond to the carbon atoms in aromatic planes, when inserted lithium diffuses to the vicinity of the interstitial carbon atoms, lithium may transfer part of its 2s electron to a nearby interstitial carbon atom, and thus result in a change of the bond between the interstitial carbon atoms and carbon atoms in aromatic planes. Lithium bonding the interstitial carbon atoms would cause a change in the relative atomic position of the interstitial carbon. These bonding changes would be activation processes, which can lead to hysteresis [14]. The present lithium insertion/de-insertion mechanism is also suitable for pyrolyzed pitch, since the microstructure of pitch pyrolyzed below 1000°C [20] is similar to that of graphite ball-milled for 150 h, except for the agglomeration of particles.

3.6. Rated capacity of ball-milled graphite electrode

Due to the interstitial carbon lowering the diffusion ability of lithium, it is expected that the rated capacity of

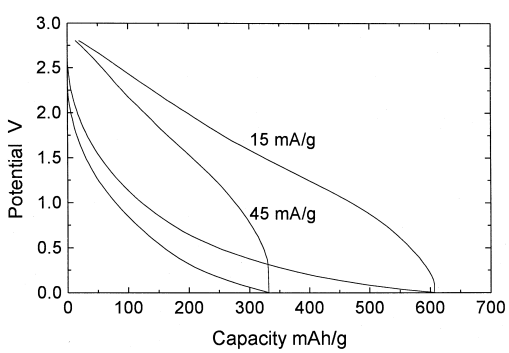

Fig. 8. Potential profiles of ball-milled graphite at different charge–discharge currents after three cycles.

ball-milled graphite is low. The potential profiles of ball-milled graphite at different charge–discharge currents are presented in Fig. 8. As the discharge current is increased from 15 to 45 mA g^{-1}, the reversible capacity decreases rapidly by 48%. In order to reveal the features of the potential plateau at different discharge currents, the dQ/dV vs. V (differential capacity) for ball-milled graphite is plotted in Fig. 9. The peak corresponding to the 1 V plateau on discharge moves to a lower potential with the decrease of discharge current. The hysteresis in the ball-milled graphite is similar to that in carbonaceous materials [38], which suggests that the reason for the hysteresis, both in ball-milled graphite and in carbonaceous materials, may be the same, and that the potential hysteresis in the two materials may be attributed to the interstitial carbon atoms between the aromatic planes of the carbon atoms.

3.7. Cycle life of ball-milled graphite electrode

The cycle life of ball-milled graphite appears to be limited. The discharge curves of ball-milled graphite for cycles 1, 2, 3, 10 and 20 are shown in Fig. 10. The capacity loss is due mainly to the elimination of the excess capacity exhibited by hysteresis, which is similar to the behaviour of pyrolyzed carbon [16]. The limited cycle life, on the one hand, may be due to some vacancies and microcavities being annihilated by moveable and bound interstitial carbons [39] during the lithium insertion and de-insertion process, which results in the carbon interstitial phases approaching each other more closely and the number of microcavities and vacancies decreasing. On the other hand, with lithium insertion and de-insertion cycling, part of the interlayers at the neck positions may be broken due to their weak connection, and electrolyte molecules may penetrate into the voids formed by the agglomerated particles. This is because the coulombic efficiency after 10 charge–discharge cycles is still about 0.96 to ~0.98, while the coulombic efficiency of unmilled graphite with the same cycling current is near to 1 after 10 charge/discharge cycles. The microstructure change during lithium insertion and de-insertion is similar to that observed for pitch coke with increasing HTTs [32].

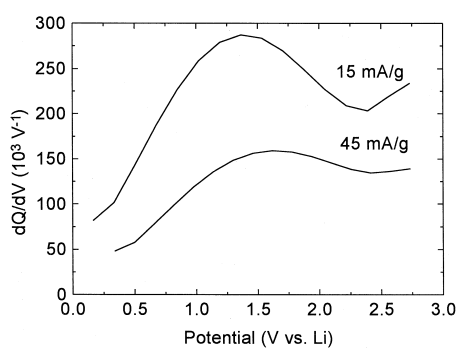

Fig. 9. Differential discharge capacity vs. potential for ball-milled graphite corresponding to Fig. 8.

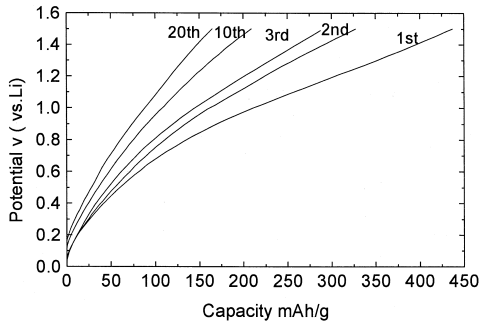

Fig. 10. Discharge curves of ball-milled graphite at cycles 1, 2, 3, 10 and 20. A cycling current of 15 mA g^{-1} was used in cycles 1–3, 10 and 20. A more-rapid cycling current of 45 mA g^{-1} was used for cycles 4–9 and 11–19.

4. Conclusions

A study has been made of the microstructure and morphology of ball-milled graphite and its electrochemical performance during lithium insertion and de-insertion. The results show that the reversible capacity of graphite ball-milled for 150 h increases up to 700 mA h g^{-1} which corresponds to 1.88 Li for 6C, which is about twice that of pristine graphite. On the other hand, the high capacity exhibits a larger potential hysteresis, and after 20 charge–discharge cycles the reversible capacity is 37.8% of its initial capacity. The capacity loss is due mainly to the elimination of the excess capacity exhibited by hysteresis, which is similar to the behaviour of pyrolyzed carbon [16]. To explain this phenomenon, we propose a mechanism whereby the large capacity of ball-milled graphite is due to lithium doped at the vacancies, microcavities (or the edges of graphene layers) and voids, as previously reported [6,10,11,37]. The potential hysteresis is attributed to the interstitial carbon atoms between the aromatic planes of the carbon atoms. The limited cycle life may be due mainly to some vacancies and microcavities being annihilated by both moveable and some bound interstitial carbon.

Acknowledgements

The authors are indebted to Professor X.B. Zhang and Dr X.Y. Song of Zhejiang University, and Professor G.L. Lu of Hangzhou University for their HREM, TEM and XRD analyses. They would also like to acknowledge the assistance of Professor H.G. Pan of Zhejiang University for the mechanical-milling of graphite used in this experiment. This work was financially supported by the National

Natural Science Foundation of China and the Natural Science Foundation of Zhejiang University.

References

[1] T. Ohzuku, Y. Iwakoshi, K. Sawai, J. Electrochem. Soc. 140 (1993) 2490.
[2] K. Tatsumui, N. Iishita, H. Sakaebe, H. Shioyama, S. Higuchi, A. Mabuchi, Fujimoto, J. Electrochem. Soc. 142 (1995) 716.
[3] T.D. Tran, J.H. Feikert, X. Song, K. Kinoshita, J. Electrochem. Soc. 142 (1995) 3297.
[4] A. Omaru, H. Azuma, M. Aoki, A. Kita, Y. Nishi, The Electrochemical Society Meeting Abstracts, Vol. 92-2, Abstract 25, Toronto, ON, Canada, Oct. 11–16, 1992, p. 34.
[5] K. Sato, M. Noguchi, A. Demachi, N. Oki, M. Endo, Science 264 (1994) 556.
[6] A. Mabuchi, K. Tokumitsu, H. Fujimoto, T. Kasuh, J. Electrochem. Soc. 142 (1995) 1041.
[7] Y. Matsumura, S. Wang, J. Mondori, Carbon 33 (1995) 1457.
[8] S. Yata, H. Kinoshita, M. Komori, N. Ando, T. Kashiwamura, T. Harada, K. Tanaka, T. Yamabe, Synth. Met. 62 (1994) 153.
[9] T. Zheng, Q. Zhong, J.R. Dahn, J. Electochem. Soc. 142 (1995) L11.
[10] K. Tokumitsu, A. Mabuchi, H. Fujimoto, T. Kasuh, J. Electrochem. Soc. 143 (1996) 2235.
[11] H.Q. Xiang, S.B. Fang, Y.Y. Jiang, J. Electrochem. Soc. 144 (1997) L187.
[12] J.S. Xue, J.R. Dahn, J. Electrochem. Soc. 142 (1995) 3668.
[13] F. Disma, L. Aymard, L. Dupont, J.-M. Tarascon, J. Electrochem. Soc. 143 (1996) 3959.
[14] J.R. Dahn, T. Zheng, Y. Liu, J.S. Xue, Science 270 (1995) 590.
[15] M. Inaba, H. Yoshido, Z. Ogumi, J. Electrochem. Soc. 143 (1996) 2572.
[16] T. Zheng, Y. Lu, E.W. Fuller, S. Tseng, V. Von Sacken, J.R. Dahn, J. Electrochem. Soc. 142 (1995) 2581.
[17] T.D. Shen, W.Q. Ge, K.Y. Wang, M.X. Quan, J.T. Wang, W.D. Wei, C.C. Koch, Nanostructured Materials 7 (1996) 393.
[18] M. Tidjani, J. Lachter, T.S. Kabre, R.H. Bragg, Carbon 24 (1986) 447.
[19] J. Piscoe, B.E. Warren, J. Appl. Phys. 13 (1942) 364.
[20] J.B. Aladekomo, R.H. Bragg, Carbon 28 (1990) 897.
[21] D.R. Maurice, T.H. Courtney, Met. Trans. 21A (1990) 289.
[22] J. Abrahamson, R.G.A. Maclagan, Carbon 22 (1984) 291.
[23] B. Pandic, in: Proceeding of the Second Conference on Industrial Carbons and Graphite, Society of Chemical Industry, Gordon and Breach, New York, 1966, p. 439.
[24] R.W. Henson, W.N. Reynolds, Carbon 3 (1965) 277.
[25] J. Lachter, R.H. Bragg, Physical Review B 33 (1986) 8903.
[26] F. Tuinstra, J.L. Koening, J. Chem. Phys. 53 (1970) 1126.
[27] M. Nakamizo, H. Honda, M. Inagaki, Carbon 16 (1978) 281.
[28] L. Nikiel, P.W. Jagodzinski, Carbon 8 (1993) 1313.
[29] T.J. Dines, D. Ttther, A. Dehbi, M. Matthens, Carbon 29 (1991) 225.
[30] R. Vidano, D.B. Fischbach, 15th Carbon Conf., Extended Abstracts, CC-1(4), p. 272, UCI, 1977.
[31] R.E. Franklin, Proc. R. Soc. London, Ser. A 209 (1951) 196.
[32] A. Oberlin, Carbon 22 (1984) 521.
[33] T. Enoki, S. Miyajima, M. Sano, H. Inokuchi, J. Mater. Res. 5 (1990) 435.
[34] W.B. Xing, J.R. Dahn, J. Electrochem. Soc. 144 (1997) 1195.
[35] Y. Matsumura, S. Wang, J. Mondori, J. Electrochem. Soc. 142 (1995) 2914.
[36] M. Pourbaix, Atlas of Electrochemical Equilibria in Aqueous Solution, NACE and CEBELCOR, 1974.
[37] K. Takei, N. Terada, K. Kumai, T. Iwahors, T. Uwai, T. Miura, J. Power Sources 55 (1995) 191.
[38] T. Zheng, W.R. Mckinnon, J.R. Dahn, J. Electrochem. Soc. 143 (1996) 2137.
[39] P.A. Thrower, R.M. Mayer, Phys. Status Solidi 47A (1978) 11.